Nonlinear Dyn (2017) 88:871–882
DOI 10.1007/s11071-016-3281-4

ORIGINAL PAPER

Fractal dimension and Wada measure revisited: no straightforward relationships in NDDS

Pranas Ziaukas · Minvydas Ragulskis

Received: 26 June 2016 / Accepted: 9 December 2016 / Published online: 21 December 2016

Abstract An extended Newton's discrete dynamical system with a complex control parameter is investigated in this paper. A novel computational algorithm is introduced for the evaluation of Wada measure. A nontrivial relationship between the fractal dimension and the Wada measure is revealed in NDDS. It is demonstrated that the reduction of the fractal dimension of basin boundaries of coexisting attractors does not automatically imply a lower Wada measure of these boundaries. Computational experiments are used to illustrate what impact the complexity of the relationship between fractal dimension and Wada measure does have in practical applications.

Keywords Chaotic attractor · Fractal dimension · Wada property

1 Introduction

Newton's discrete dynamical system Newton's discrete dynamical system (NDDS) is a paradigmatic model used to illustrate the fractality in nonlinear dynamical systems. Newton's method is used to compute complex basins of attraction for different discrete nonlinear dynamical systems in [16]. The chaotic number of iterations needed by Newton's method to converge to its attractors is discussed in [29]. A general behavior of Newton's method for cubic polynomials is investigated in [33], including the emergence of period-three orbits.

The emergence of fractals in NDDS is a well-known effect studied by many researchers. The overview of NDDS and the convergence to fractal patterns is given in [18]. Theoretical and experimental evidence of fractal characteristics of NDDS is presented in [28]. Some peculiar examples of fractals obtained using NDDS are presented in [6]. The theory for the stabilization of NDDS in order to eliminate fractal basin boundaries is developed in [10]. Implications of the fractal basin boundaries generated by NDDS for the aeroelastic analysis of a helicopter motion are discussed in [8].

It is well known that NDDS basins of attraction can become very complex. An in-depth analysis of interwoven basins of attraction using a damped Newton's method is discussed in [12]. A graphical representation of interlacement among three different basins of attraction in NDDS is presented in [14]. A variety of alternatives and modifications to NDDS are known. A modification of NDDS using a novel adaptive step size control procedure is proposed in [2]. Standard Newton's method, Halley's method and Schroder's method are compared in terms of structural characteristics of

P. Ziaukas · M. Ragulskis (✉)
Department of Mathematical Modeling, Kaunas University of Technology, Kaunas, Lithuania
e-mail: minvydas.ragulskis@ktu.lt

P. Ziaukas
e-mail: pranas.ziaukas@ktu.edu

Julia sets in [34]. A variety of different possible generalizations of NDDS is reviewed in [15].

Wada property Wada property emerges in a variety of systems and attracts lots of interest in nonlinear physics. Rigorous theorems and important statements regarding Wada basin boundaries and basin cells are presented in [22]. Wada property for different types of attractors including strange non-chaotic attractors is discussed in [35]. Sufficient and necessary conditions guaranteeing that three Wada basins are emerging from a tangent-type bifurcation are presented in [5].

Wada property in chaotic scattering systems with multiple exit modes is analyzed in [24]. Topological characteristics, including Wada property, are considered for a system with chaotic scattering in [30]. The unpredictable behavior of Wada basin boundaries in the Duffing oscillator is noted in [1]. Wada exit basin boundaries are analyzed in a tokamak system in [25]. Seemingly unexpected situations where basins of attraction have Wada property are revealed in [19]. Unpredictability of ecological models related to Wada basins is interpreted graphically in [31]. Examples of Wada characteristic in a periodically forced Lotka–Volterra predator–prey model are found in [32]. Transitions from totally Wada basins to partially Wada basins and vice versa are constructed in [36]. A novel method for testing for basins of Wada is proposed in [9].

2 Newton's discrete dynamical system

Basic Newton's method (also known as the Newton–Raphson method) is a paradigmatic method for finding roots of a real-valued polynomial $p(x)$ [3].

After the method was established in the seventeenth century, modern interpretations and implementations began to differ substantially from the original version.

In the nineteenth century, Schrder [27] and Cayley [7] came up with problems and solutions that eventually led to the formal generalization of the Newton's method for a polynomial $p(z)$ with complex coefficients. In this work, it is referred to as the Newton's discrete dynamical system.

2.1 The concept

Definition Newton's dynamical system $f : \mathbb{C} \to \mathbb{C}$ is a discrete dynamical system fully described by its iterations $z_{k+1} = f(z_k)$, where $z_k, z_{k+1} \in \mathbb{C}$. For a given complex polynomial $p(z)$, a single Newton's iteration at a point $z \in \mathbb{C}$ is defined as

$$f_p(z) = z - \frac{p(z)}{p'(z)}. \tag{1}$$

Once the evolutionary process is fully described, NDDS (corresponding to some complex polynomial $p(z)$) can be considered; the behavior of this dynamical system is characterized by orbits $\{ z_0, z_1, z_2, \dots \}$. Each orbit is determined by the initial seed $z_0 \in \mathbb{C}$:

$$z_n = f_p^{\circ n}(z_0), \quad \forall n \in \mathbb{N}. \tag{2}$$

Without the loss of generality, the third degree polynomial $p(z) = z^3 - 1$ is considered further in this paper.

Basins of attraction $\mathscr{B}_k$, $k \in \{ 1, 2, 3 \}$, for $p(z) = z^3 - 1$ are illustrated in Fig. 1. It is known that the system has exactly three attractors [11] under these circumstances: $z = 1$ (color blue), $z = e^{2\pi/3}$ (color red) and $z = e^{4\pi/3}$ (color yellow). The closest attractor is assigned to an initial seed $z_0 \in \mathbb{C}$ after $n = 30$ iterations. It is apparent that the basins are intertwined in a complex manner. Basins of attractions for higher order polynomials $p(z) = z^4 - z$ and $p(z) = z^5 - 1$ are illustrated in Fig. 2.

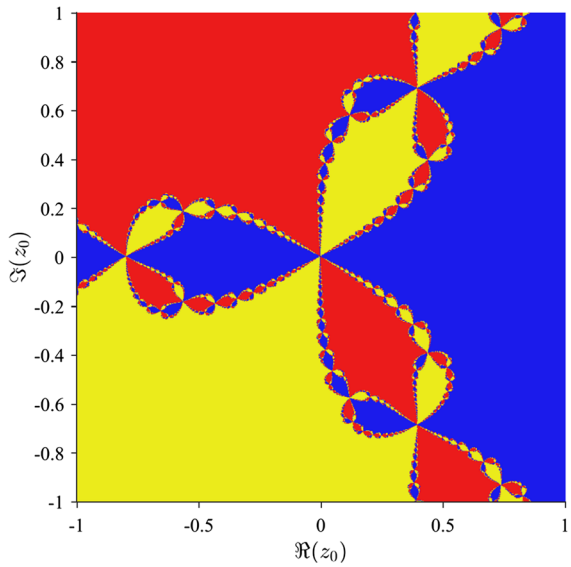

Fig. 1 Basins of attraction for the NDDS with $p(z) = z^3 - 1$. Each *color* corresponds to the different attractor $\mathscr{A}_k$, where $k \in \{ 1, 2, 3 \}$

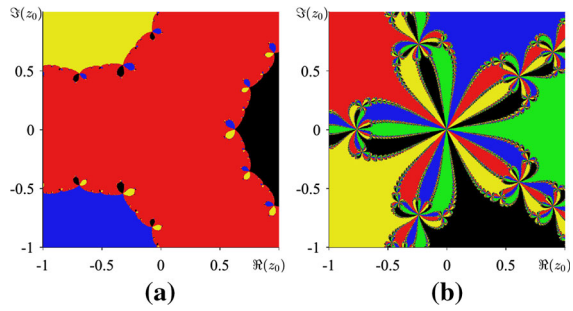

Fig. 2 Basins of attraction for the NDDS with polynomials of higher order. Different polynomials $p(z)$ are used. **a** $p(z) = z^4 - z$; **b** $p(z) = z^5 - 1$

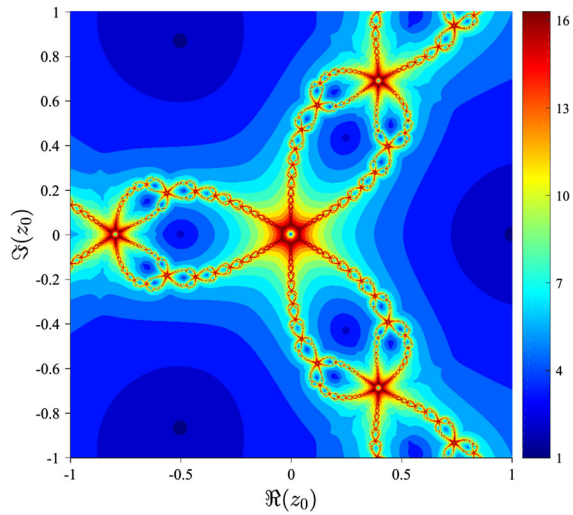

Fig. 3 The speed of convergence of NDDS with $p(z) = z^3 - 1$ measured in terms of H-ranks

Attractors NDDS f_p has a set of attractors $\mathscr{A} \subset \mathbb{C}$, comprised of the fixed points satisfying the definition $\{r \in \mathbb{C} \mid p(r) = 0\}$. Consequently, it is important to understand the basins of attraction $\mathscr{B}$ for each attractor—the structure, properties and dynamics of these peculiar sets [11].

Speed of convergence Another important aspect is the speed of convergence of trajectories to appropriate attractors. It is shown in [21] that clocking convergence to complex and chaotic attractors may reveal important dynamic characteristics of the investigated nonlinear systems. The speed of convergence is measured in terms of H-ranks and presented in Fig. 3 for NDDS with $p(z) = z^3 - 1$. It can be observed that H-ranks are substantially higher in the vicinities of the basin boundaries $\partial\mathscr{B}$. It can be seen that NDDS is very sensitive to the selection of initial conditions around these boundaries.

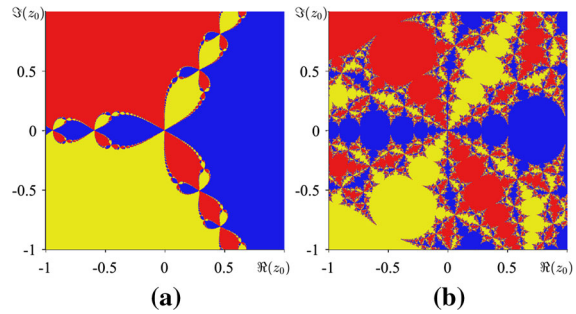

Fig. 4 Basins of attraction for the generalized NDDS with $p(z) = z^3 - 1$. Different parameters $\alpha \in \mathbb{R}$ are used. **a** $\alpha = 0.5$; **b** $\alpha = 2$

2.2 Generalization

It is shown in [16] that typical speed of convergence of NDDS varies depending on initial conditions. In order to improve the convergence of NDDS, the following generalization is introduced in [15]

$$f_p(z) = z - \alpha \frac{p(z)}{p'(z)}; \tag{3}$$

where $\alpha \in \mathbb{C}$. The modified Newtonian iteration (3) introduces an arbitrary coefficient $\alpha \in \mathbb{C}$ instead of a constant value $\alpha = 1$.

This generalization of NDDS introduces a quantitative change in the speed of convergence as well as a qualitative change in the basins of attraction for the NDDS for $\alpha \in \mathbb{R}$. Typically $0 < \alpha < 1$ softens the fractal pattern of the basin boundary (see Fig. 4a). On the other hand, $\alpha > 1$ typically sharpens the fractal pattern while providing bigger and more aggressive changes in the system variable z_k (see Fig. 4b).

3 Fractal dimension of NDDS

3.1 The concept of the algorithm

The fractal dimension of a set provides an objective mean to compare different sets in terms of their complexity. Box counting dimension (also known as

Minkowski or Minkowski–Bouligand dimension) provides a way of determining the fractal dimension of a set $\mathscr{F}$ in any metric space.

A two-dimensional square box of side length ε around the point $z_0 \in \mathbb{C}$ is defined as

$$B(\varepsilon, z_0) = \left\{ z \in \mathbb{C} \,\middle|\, \Re(z_0) - \frac{\varepsilon}{2} \le \Re(z) \le \Re(z_0) + \frac{\varepsilon}{2}, \; \Im(z_0) - \frac{\varepsilon}{2} \le \Im(z) \le \Im(z_0) + \frac{\varepsilon}{2} \right\}. \quad (4)$$

The box defined above is actually a closed ball described using Manhattan metric [20] instead of a more typical Euclidean one. Nevertheless, it is useful when working in discrete grids which typically occur in computational environments. Note that such definition of ε-surrounding is much more computationally efficient according to [26].

The minimal number of boxes of side length ε that are needed to cover a given closed and compact set $\mathscr{F}$ is denoted as

$$N(\varepsilon) = \min \left\{ n \in \mathbb{N} \,\middle|\, \mathscr{F} \subset \bigcup_{k=1}^{n} B(\varepsilon, z_k), z_k \in \mathbb{C} \right\}. \quad (5)$$

Such a number $N(\varepsilon)$ can always be found in case of $\mathscr{F}$ being compact because it follows from the very definition of the compactness (that there exists a finite subcover of open balls). Among these finite coverings, some (or at least one) are minimal.

Now the dimension D of fractal $\mathscr{F}$ is related to the number N such that

$$N(\varepsilon) \approx C\varepsilon^{-D}, \quad \text{for some } C > 0; \quad (6)$$

and the above approximation becomes more precise as ε decreases [4]. Then D can be expressed as follows

$$D(\mathscr{F}) = \lim_{\varepsilon \to 0} \frac{\log N(\varepsilon)}{\log(1/\varepsilon)}; \quad (7)$$

where $N(\varepsilon)$ is the number of ε-sized boxes that are required to cover $\mathscr{F}$.

3.2 The fractal dimension algorithm for the NDDS

The basic idea of the algorithm is based on scanning a nonoverlapping ε-sized grid, finding the portions containing $\mathscr{F}$ (see Fig. 5) and making conclusions according to the definition of box counting dimension.

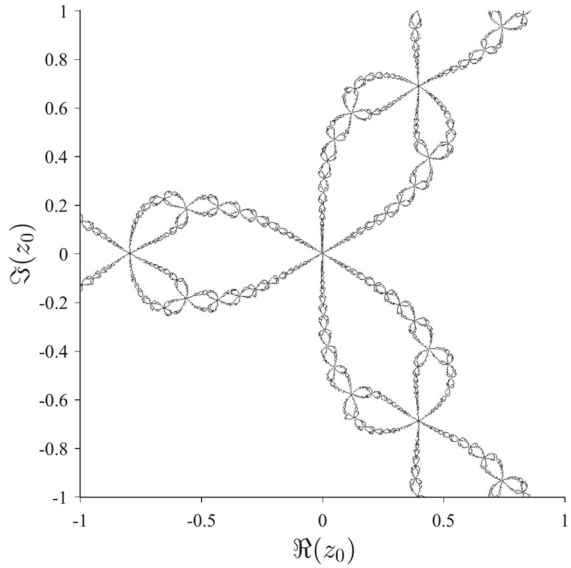

Fig. 5 Basin boundary $\mathscr{F} = \partial\mathscr{B}$ for the NDDS with $p(z) = z^3 - 1$ and $\alpha = 1$

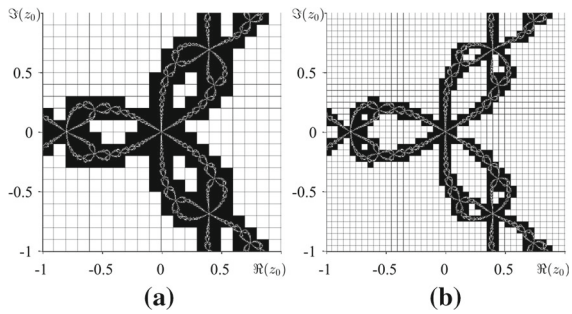

Fig. 6 The principle of box counting using boxes of various sizes ε. The digital representation of $\mathscr{F}$ is split into an ε-grid. The algorithm counts the nodes where the basin boundary $\partial\mathscr{B}$ is present. **a** $\varepsilon = 0.1$; $N(\varepsilon) = 145$; **b** $\varepsilon = 0.05$; $N(\varepsilon) = 355$

In reality, the ability to reduce ε is limited. For digital images (the representation of fractal structures), it is not possible to zoom more than to an individual pixel (given a single fixed image, the basin boundary is also fixed). The algorithm is comprised of the following steps:

1. Consider some finest $\varepsilon \in S$ values.
   These should initially cover 1×1 grid of pixels, then 2×2 grid pixels and so on (see Fig. 6).
2. Compute the trend $\log N(\varepsilon)$, and $\log(1/\varepsilon)$ in each case.
   The definition of N is applied.

3. Approximate the slope using the least square linear regression.
   Assume that some pairs of observations (x_k, y_k), $k = \overline{1, \ldots, n}$ are supposed to be related $y_k = \gamma x_k + C$ up to some level of accuracy. Here γ is the slope, and C is a constant. Then the evaluation that minimizes root-mean-square error (RMSE) is

$$\gamma(x, y) = \frac{n \sum_{k=1}^{n}(x_k y_k) - \left(\sum_{k=1}^{n} x_k\right)\left(\sum_{k=1}^{n} y_k\right)}{n \sum_{k=1}^{n} x_k^2 - \left(\sum_{k=1}^{n} x_k\right)^2}. \tag{8}$$

Finally, the approximation of fractal dimension D can be expressed

$$D(\mathscr{F}) \approx \gamma(\log(1/\varepsilon), \log N(\varepsilon)). \tag{9}$$

This algorithm is used to compute fractal dimensions of basin boundaries of NDDS in this paper.

4 Wada measure

4.1 A basic illustration

In theoretical mathematics and physics, there exists a concept called lakes of Wada [19]. This phenomenon occurs in a plane which is divided into at least three disjoint connected open sets that have a peculiar but highly counter-intuitive property: They all share the same boundary.

Let us construct a region that has Wada property. For clarity, three different basins of attraction are denoted as R, Y and B (the basins correspond to red, yellow and blue colors, respectively).

1. Without a loss of generality, it can be assumed that the region is rectangular.
   Initially all points in the region are undefined (not assigned to any basin of attraction).
2. The undefined region is divided vertically into three equal parts.
   Side parts are assigned to two different basins of attraction; the middle part is left undefined.
3. The undefined parts are divided vertically into three equal even smaller parts.
   Side parts are left undefined; the middle part is assigned to the basin which is not nearby.
4. Step 3 is repeated indefinitely.

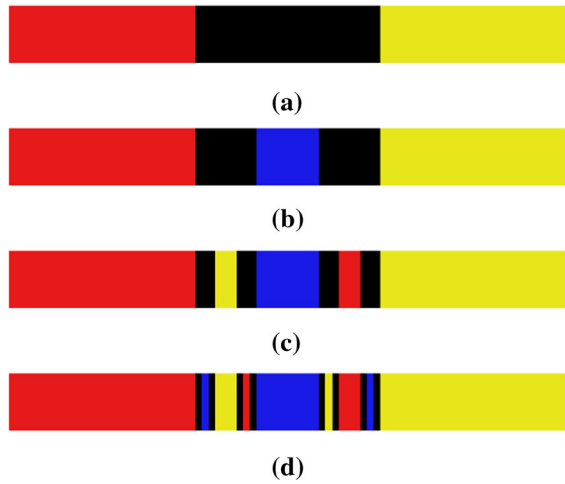

Fig. 7 Emergence of Wada property. A region is divided into three pieces; side pieces are assigned to two different basins of attraction, and the middle piece is left undefined. An undefined portion is again divided into three pieces in every subsequent turn; side pieces are undefined; the middle piece is assigned to the basin of attraction which is not in the neighborhood

As the number of repeated iterations n increases, the set of undefined points is getting smaller. In the limit case $n \to +\infty$, a whole region of points is assigned to some basins R, Y and B. Moreover, all these basins have a common boundary, thus the Wada property. The whole process is illustrated in Fig. 7.

4.2 The concept of the algorithm

As discussed previously, the situation when every boundary point neighbors more than two distinct basins of attraction $\mathscr{B}_k$, $k \in \overline{1, \ldots, n}$ is known as the Wada property. If the system has exactly three different attractors $\mathscr{A}_1$, $\mathscr{A}_2$, $\mathscr{A}_3$, it follows that all basins of attraction $\mathscr{B}_1$, $\mathscr{B}_2$, $\mathscr{B}_3$ have a common boundary $\partial\mathscr{B}$. Some more preliminary definitions are needed before proceeding with quantitative approximations of Wada measure.

The number of n-boxes $N_n(\varepsilon)$ is the minimal number of boxes (according to the definition of N) that satisfy an additional property

$$B(\varepsilon, z) \cap \mathscr{B}_k \neq \emptyset, \quad \text{for all } k \in \{k_1, k_2, \ldots, k_n\}; \tag{10}$$

for a fixed side length ε and compact nonempty set $\mathscr{F}$.

Simply put, the number of n-boxes counts the size of (partial) $\mathscr{F}$ covering which contains points from at least n different basins of attraction. Then the following inequality holds

$$0 \leq N_n(\varepsilon) \leq N(\varepsilon), \quad \forall n \in \mathbb{N}, \ \forall \varepsilon > 0. \tag{11}$$

Let us look at the case where a given dynamical system has exactly three attractors and three corresponding basins of attraction $\mathscr{B}_1$, $\mathscr{B}_2$, $\mathscr{B}_3$ more closely. In extreme cases where the basins are relatively far away and boundaries are distinct, it is reasonable to expect $N_3(\varepsilon) \approx 0$, whereas if basins are intertwined and close together, it follows that $N_3(\varepsilon) \approx N(\varepsilon)$.

Finally, the Wada measure can be rigorously defined. A Wada measure W for a compact nonempty set $\mathscr{F} \subset \mathbb{C}$ is defined as

$$W(\mathscr{F}) = \lim_{\varepsilon \to 0} \frac{N_3(\varepsilon)}{N_2(\varepsilon)} = \lim_{\varepsilon \to 0} \frac{N_3(\varepsilon)}{N(\varepsilon)} \tag{12}$$

where $N(\varepsilon)$ and $N_3(\varepsilon)$ are the number of ε-sized boxes that cover $\mathscr{F}$.

In terms of the classical theory of probability, the Wada measure is the probability of a random point taken from boundary $\partial\mathscr{B}$ having at least three different basins of attraction in its immediate neighborhood. If the region of interest has full Wada property, then its boundary $\partial\mathscr{B}$ has a theoretical Wada measure $W(\partial\mathscr{B}) = 1$. On the contrary, if the region does not resemble Wada situation at all, then $W(\partial\mathscr{B}) = 0$.

4.3 The Wada algorithm for NDDS

Once again, the idea involves scanning a nonoverlapping ε-sized grid, finding the portions containing $\mathscr{F}$, counting the number of basins of attraction that they contain and making conclusions according to the definition of Wada measure.

The ability to reduce ε is similarly limited to no more than an individual pixel. The proposed algorithm reads:

1. Assign finest possible values $\varepsilon \in S$.
   These should initially cover 2×2 grid of pixels, then 3×3 grid pixels and so on (see Fig. 8).
2. Calculate the observations $N(\varepsilon)$ and $N_3(\varepsilon)$ in each case.
   The empirical probability for any given box (being it a 3-box) is $N_3(\varepsilon)/N(\varepsilon)$.

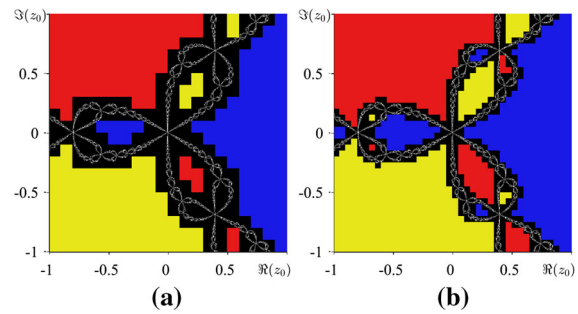

Fig. 8 The principle of Wada measure using boxes of various sizes ε. The digital representation of $\mathscr{F}$ is split into an ε-grid, and then count the nodes where the basin boundary $\partial\mathscr{B}$ is present and count the occurrences from different basins of attraction. **a** $\varepsilon = 0.1$; $N_3(\varepsilon) = 143$; $N(\varepsilon) = 145$; **b** $\varepsilon = 0.05$; $N_3(\varepsilon) = 342$; $N(\varepsilon) = 355$

3. Compute the mean empirical probability of the observations.

   The outcome of the proposed algorithm yields

$$W(\mathscr{F}) \approx \frac{1}{|S|} \sum_{\varepsilon \in S} \frac{N_3(\varepsilon)}{N(\varepsilon)}. \tag{13}$$

Realistically, the approximated value of $W(\mathscr{F})$ is never quite equal to 1. On the other hand, it serves its purpose of measuring and comparing Wada characteristics of different dynamical systems and situations. This approximation is used in further analysis of NDDS.

5 Basin boundaries of NDDS

Computationally reconstructed visual representations of attractors and basins of attraction are among typical choices for researchers who seek to describe and analyze the behavior of some dynamical systems [23]. Therefore, it is important to do a qualitative analysis of characteristics, relationships between these characteristics, and possible implications of these results.

Initial conditions $z_0 \in \mathbb{C}_1$ are further considered ($\mathbb{C}_1 = [-1, 1]^2$). This set includes all attractors for the NDDS with polynomial $p(z) = z^3 - 1$. The resolution of initial conditions is set to $|\Delta z| = 0.0025$; a 801×801-sized grid of initial values for z_0 is considered.

Similarly, we select a 201×201 grid of possible values for $\alpha \in \mathbb{C}_1$; $|\Delta\alpha| = 0.01$. It can be noted that such variation of α is sufficient for the qualitative analysis

of NDDS behavior—the variation of z_k becomes too rapid outside this region.

The number of iterations used in the model is set to $n = 30$. The evolution of a trajectory $((z_0, z_1, z_2, \ldots, z_{30}))$ is terminated at z_{30}, and the orbit is assigned to the nearest attractor $\mathscr{A}$.

5.1 Fractal dimensions of NDDS boundaries

Different coverings ranging from 1×1 to 100×100 pixels are used in the algorithm for the reconstruction of fractal dimensions of NDDS boundaries ($|S| = 100$).

In general, a fractal dimension D is a characteristic of complexity comparing how details of a pattern change with the scale at which it is being measured. For smooth simple curves, this characteristic is a constant unit $D = 1$ (meaning that there is no change in detail).

Let us consider the parameter value $\alpha = -0.55 + 0.6i$. We use NDDS to construct basins of attraction $\mathscr{B}$, basin boundary $\partial\mathscr{B} = \mathscr{F}$, and finally the reconstruction of fractal dimension yields $D(\mathscr{F}_\alpha) = 1.21$. However, results become quite different at $\alpha = 0.5 + 0.9i$ where fractal dimension is $D(\mathscr{F}_\alpha) = 1.63$. This difference in fractal dimensions can be also clearly observed visually (Fig. 9). Such a difference between fractal dimensions of the two images of basin boundaries requires a more detailed investigation.

The variation of the fractal dimension of NDDS in respect of α when $0 \le \alpha \le 1$ is illustrated in Fig. 10a. It is interesting to note that $D(\mathscr{F}_0) \approx 1$—but the fractal dimension increases almost monotonically as α tends to 1. On the contrary, the variation of the fractal dimension

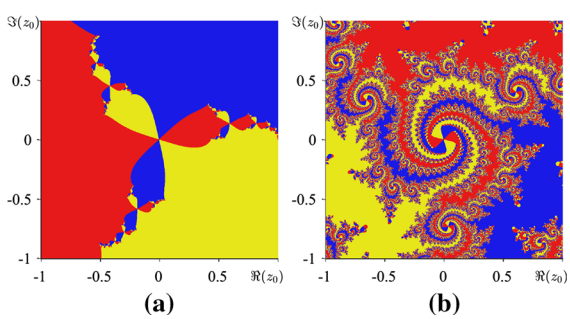

Fig. 9 Basins of attraction and the fractal dimensions for the NDDS. **a** $\alpha = -0.55 + 0.6i$; $D(\mathscr{F}_\alpha) = 1.21$; **b** $\alpha = 0.5 + 0.9i$; $D(\mathscr{F}_\alpha) = 1.63$

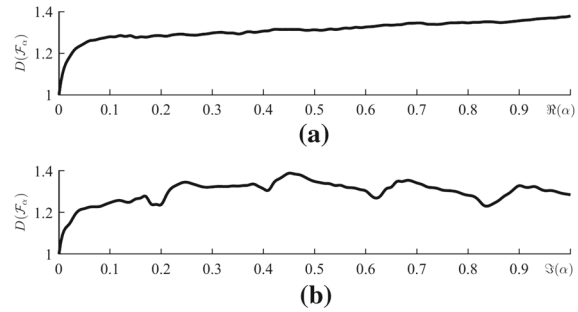

Fig. 10 Fractal dimensions for the NDDS with varying parameter $\alpha \in \mathbb{C}$. **a** $\alpha \in [0, 1]$; **b** $\alpha \in [0, 1]i$

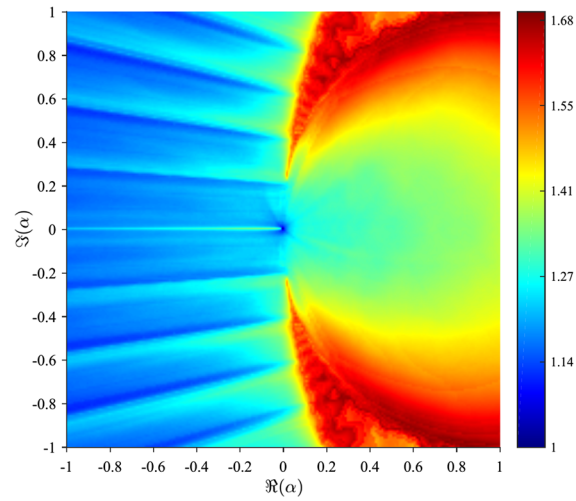

Fig. 11 Fractal dimension $D(\mathscr{F}_\alpha)$ in the parameter plane $\alpha \in \mathbb{C}$

in respect of α when $\alpha \in [0, 1]i$ is far from being monotonic (see Fig. 10b).

The whole complexity of this relationship is revealed in Fig. 11. It appears that the fractal dimension D is a highly nontrivial and non-monotonic function of complex parameter $\alpha \in \mathbb{C}$. It is interesting to note that the image in Fig. 11 is symmetric with respect to the line $\Im(\alpha) = 0$.

For $\Re(\alpha) \le 0$, the fractal dimension of NDDS is relatively low, with the maximum located at $D(\mathscr{F}_{0.45i}) \approx 1.39$ and the minimum at $D(\mathscr{F}_0) \approx 1$. An almost periodic variation of the fractal dimension along the imaginary axis can be also observed in this semi-plane.

The variation of the fractal dimension is completely different in the semi-plane $\Re(\alpha) \ge 0$; the periodic behavior is not present here. However, the

fractal dimension increases dramatically as the $\Im(\alpha)$ approaches ± 1.

5.2 Wada measures of NDDS boundaries

Different coverings ranging from 2×2 to 101×101 pixels are used in the algorithm (the single pixel case is trivial) for the reconstruction of Wada measures of NDDS boundaries.

Wada measure W indicates what percentage of boundary points $\mathscr{F}$ is neighboring more than two basins of attraction simultaneously; $W = 0$ corresponds to 0%, while $W = 1$ corresponds to 100%.

Consider a particular parameter $\alpha = -0.85 + 0.53i$. We use NDDS to obtain the basins of attraction $\mathscr{B}$, basin boundary $\partial\mathscr{B} = \mathscr{F}$, and finally the reconstructed Wada measure is $W(\mathscr{F}_\alpha) = 0.28$. This result is very different from $\alpha = 0.1 + 0.6i$, and the corresponding Wada measure $W(\mathscr{F}_\alpha) = 0.88$. The visual comparison is presented in Fig. 12.

As the parameter α takes values $0 \leq \alpha \leq 1$, the changes in Wada measure are inspected. Initially $W(\mathscr{F}_0) \approx 0$, but the measure increases rapidly (for example, $W(\mathscr{F}_{0.03}) \approx 0.91$) and remains $W > 0.9$ afterward. This variation is illustrated in Fig. 13a. In another scenario, $\alpha \in [0, 1]i$ and the resulting Wada measures reveal a periodic-like behavior (see Fig. 13b).

Wada measures for the whole grid of parameter values $\alpha \in \mathbb{C}_1$ are presented in Fig. 14. It appears that the Wada measure W is a nontrivial function of complex parameter $\alpha \in \mathbb{C}$.

For $\Re(\alpha) \leq 0$, the Wada measures vary significantly within $W \in [0.03, 0.90]$. The average measure

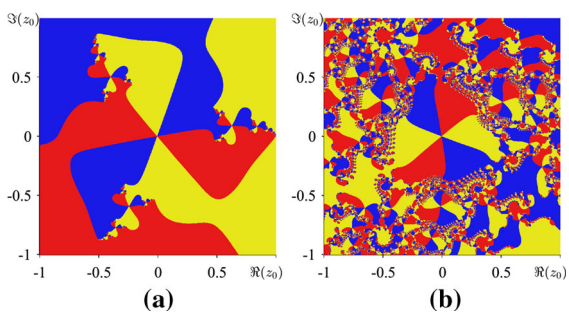

Fig. 12 Basins of attraction and the Wada measures for the NDDS. **a** $\alpha = -0.85 + 0.53i$; $W(\mathscr{F}_\alpha) = 0.28$; **b** $\alpha = 0.1 + 0.6i$; $W(\mathscr{F}_\alpha) = 0.88$

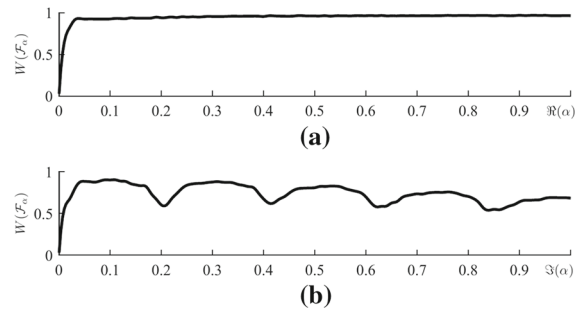

Fig. 13 Wada measures for the NDDS with varying parameter $\alpha \in \mathbb{C}$. **a** $\alpha \in [0, 1]$; **b** $\alpha \in [0, 1]i$

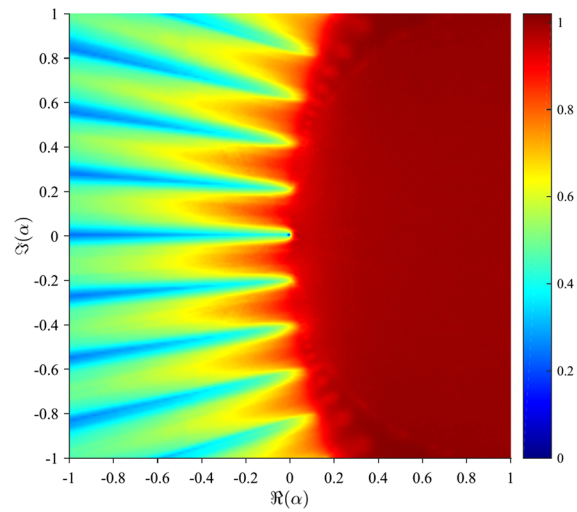

Fig. 14 Wada measure $W(\mathscr{F}_\alpha)$ in the parameter plane $\alpha \in \mathbb{C}$

in this case is $\overline{W} \approx 0.53$. The periodic-like behavior along imaginary axis is present only in this semiplane.

On the other hand, for $\Re(\alpha) \geq 0$ the measures are relatively high. The highest observed value is $W(\mathscr{F}_{0.59-i}) \approx 0.99$. The values are high almost everywhere (except for $\Re(\alpha) \approx 0$) with average being $\overline{W} \approx 0.94$.

5.3 The relationship between the fractal dimension and Wada features

Figures 11 and 14 (representing the variation of the fractal dimension and Wada features accordingly) are somewhat similar in the shape—however, principal differences exist between these two figures. These differences are clearly illustrated in the phase plane

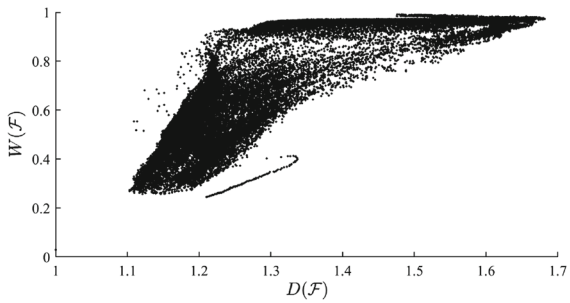

Fig. 15 Fractal dimensions $D(\mathscr{F})$ and Wada measures $W(\mathscr{F})$ for all parameters $\alpha \in \mathbb{C}_1$

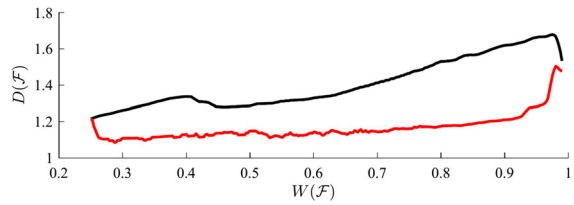

Fig. 16 Minimum and maximum fractal dimensions for the ε-neighborhoods of a fixed Wada measure $W(\mathscr{F})$

$D(\mathscr{F}) - W(\mathscr{F})$ (Fig. 15). We run through all discrete values of α ($\alpha \in [-1, 1]^2$)—and for each α, we plot a dot in the phase plane $D(\mathscr{F}) - W(\mathscr{F})$. In other words, we do not visualize the variation of α—but the relationship between $D(\mathscr{F})$ and $W(\mathscr{F})$. If this relationship would be linear, the points in Fig. 15 should be scattered around an incline line. However, it is clear that this relationship is much more complex (see Fig. 15).

Strictly speaking, the geometric distribution of points in Fig. 15 could suggest some positive correlation between $D(\mathscr{F})$ and $W(\mathscr{F})$. Indeed, Pearson's correlation coefficient [17] (without checking the normality of the distribution and assuming only finite (co)variances) suggests a positive correlation: $\rho_{D,W} = 0.82$. At the same time, the Spearman's correlation coefficient $r_{D,W} = \rho_{\text{rank}(D),\text{rank}(W)} = 0.87$. Because of the ranking feature, this measure is relatively robust to outliers (unlike Pearson's correlation) [17].

However, despite some positive correlation the relationship between $D(\mathscr{F})$ and $W(\mathscr{F})$ is still complex. It is possible to provide a sequence of fractal basin boundaries whose dimension D strictly increases, yet at the same time, the corresponding Wada measure decreases. The aforementioned effect can be demonstrated in the scatter plot (see Fig. 15) by selecting a negatively correlated subset of observations ($\rho_{D,W} \approx -1$).

Figure 16 reveals another aspect of this relationship. Let us fix a particular Wada measure W. Now, for an ε-environment of this fixed Wada measure (note that parameter α is not fixed in this computational experiment) we seek all possible fractal dimensions. The minimum fractal dimension is shown in red, the maximum—in black (Fig. 16). Both lines (the red and the black) intersect at $W(\mathscr{F}) \approx 0.244$. This is because there exists only one single parameter $\alpha = -1$ where $W(\mathscr{F}) = 0.244$ and $D(\mathscr{F}) = 1.21$.

Figure 16 proves again, in an alternative way, that the relationship between $D(\mathscr{F})$ and $W(\mathscr{F})$ is very complex. High fractal dimension does not necessarily imply a high Wada feature—and vice versa.

It is very well known that the reduction of the fractal dimension of basin boundaries of coexisting attractors can be useful for attractor control applications. A typical example can be found in [13] where the elimination of fractal boundaries between basins of coexisting attractors helps to control a dendritic neuron with phase-independent stimulation. However, computational experiments with NDDS reveal counter-intuitive results.

Let us assume that the fractal dimension of NDDS basin boundaries is 1.6. Then, according to Fig. 16, Wada measure of these boundaries can vary in the interval between 0.88 and 0.98. Let us consider that one does manage to decrease the fractal dimension of the boundaries down to 1.25 (by perturbing the control parameter α). But it appears that Wada measure of the perturbed system can be anywhere in the interval between 0.29 and 0.93 (Fig. 16). As mentioned previously, this is a strongly counter-intuitive result. It may happen that the fractal dimension of the perturbed system is 1.25 and Wada feature is 0.93. One could assume that decreasing the fractal dimension from 1.6 to 1.25 could substantially improve the controllability of the convergence processes to required attractors. However, one should assess not only the fractal dimension D. It may appear that high Wada measure W does prevent the ability to improve the controllability of attractors—even though the fractal dimension of boundaries is considerably decreased.

Table 1 Distribution of simulations (out of $s = 795$) that approach different attractors $\mathscr{A}_1$, $\mathscr{A}_2$, $\mathscr{A}_3$ under various values of parameter α

α	$s(\mathscr{A}_1)$	$s(\mathscr{A}_2)$	$s(\mathscr{A}_3)$
0.97	136	136	523
1	268	268	259
$1 + 0.005i$	261	472	62

6 Uncertainty of the convergence to the final attractor

6.1 Computational experiment #1

Let us construct a set of initial conditions in a disk; the center of the disk is set to $z_0 = -0.793$, and the radius of the disk is $|\Delta z_0| = 0.01$. Seven hundred and ninety-five discrete points representing different initial conditions are uniformly distributed in the disk (the average distance between adjacent points of initial conditions in the complex plane is 0.0006).

Initially, the control parameter α is set to 0.97. It appears that in 523 cases from 795, the trajectories of NDDS converge to attractor $\mathscr{A}_3$. One hundred and thirty-six trajectories converge to attractor $\mathscr{A}_1$; other 136 trajectories—to attractor $\mathscr{A}_2$ (Table 1).

Next the control parameter α is set to 1. Computational simulations reveal that the number of trajectories attracted to different attractors is now almost the same: 268 trajectories converged to $\mathscr{A}_1$, 268—to $\mathscr{A}_2$, and 259—to $\mathscr{A}_3$. Finally, the control parameter α is set to $1 + 0.005i$. Two hundred and sixty-one trajectories converged to $\mathscr{A}_1$, 472—to $\mathscr{A}_2$, and 62—to $\mathscr{A}_3$ (Table 1).

These computational results do demonstrate that for a system with the Wada property, it is important to consider not only the boundary itself (in terms of fractal dimension), but also the neighboring basins of attraction (in terms of Wada measure).

6.2 Computational experiment #2

Let us consider three initial conditions z_0: $-0.793 - 0.001i$, -0.793 and $-0.793 + 0.001i$. Also, let us consider two values of the control parameter α: 1 and 0.99.

In order to simplify the visualization of transient processes, we plot only the arguments of the points in each trajectory. Strictly speaking, the convergence of arguments does not ensure the convergence of a trajectory to an appropriate attractor—this aspect is checked separately after the termination of each trajectory.

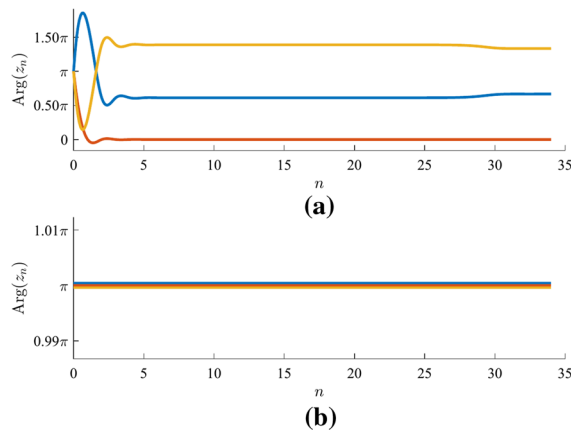

Fig. 17 Trajectories of the NDDS orbits when the initial seed $z_0 = -0.793$ varies by $\Delta z = 0.001i$ and the parameter α is slightly perturbed. **a** $\alpha = 1$; **b** $\alpha = 0.99$

Note that the arguments of all three different initial conditions are almost the same ($\approx\pi$). Arguments of all three trajectories quickly separate and converge to distinct values (Fig. 17a). In fact, these argument values correspond to the three distinct attractors $\mathscr{A}_1$, $\mathscr{A}_2$, $\mathscr{A}_3$.

Now, the control parameter α is perturbed to 0.99. It appears that this perturbation, though slight is critical. Arguments of all three trajectories immediately converge to π and remain unchanged during the whole computation process (Fig. 17b).

The fact that the convergence of the system can be completely altered by a small perturbation of a control parameter is not an astonishing fact. However, the ability to predict the convergence of a trajectory started from an arbitrary initial condition is influenced not only by the positioning and the complexity of the basin boundary—but also by the intertwining of the basins themselves. That intertwining of more than two basins cannot be measured by the fractal dimension of the basin boundary—it requires an algorithm capable to measure the Wada property.

7 Concluding remarks

A novel algorithm for computing Wada measure W is proposed in this paper. This algorithm evaluates the limited precision of computations and is applicable for

assessing Wada measure of data produced by experimental observations (when it is not possible to zoom in order to obtain a more detailed picture of the model). Wada measure is computed using different scales of the observation window (down to a single pixel) without iterative repetitive recomputation of basins of attraction at every different scale. Such an approach enables efficient and accurate reconstruction of Wada measure in the parameter plane and mimics the scaling feature used in the fractal dimension computation algorithm. Wada measure is computed for all grid points of the parameter plane at different scales of granularity.

It is demonstrated that there does not exist a straightforward relationship between the fractal dimension D and Wada measure W. From one point of view, this is not a very astonishing fact—the proposed Wada algorithm takes into account more data compared to the fractal dimension algorithm. On the other hand, computational experiments with NDDS reveal surprising results.

It is well known that transient processes produced by NDDS can be used to illustrate results of iterative root finding algorithms for nonlinear equalities [7,11]. However, the unpredictability of transient processes governed by Wada boundaries of coexisting attractors suggests interesting potential applications also in the area of attractor control techniques. Control applications of coexisting attractors in different nonlinear dynamical systems by utilizing Wada measures are a definite topic for future research.

Acknowledgements Financial support from the Lithuanian Science Council under project no. MIP078/15 is acknowledged.

References

1. Aguirre, J., Sanjuán, M.A.: Unpredictable behavior in the Duffing oscillator: Wada basins. Phys. D: Nonlinear Phenom. **171**(1–2), 41–51 (2002). doi:10.1016/S0167-2789(02)00565-1
2. Amrein, M., Wihler, T.P.: An adaptive Newton-method based on a dynamical systems approach. Commun. Nonlinear Sci. Numer. Simul. **19**(9), 2958–2973 (2014). doi:10.1016/j.cnsns.2014.02.010
3. Atkinson, K.E.: An Introduction to Numerical Analysis. Wiley, Hoboken (1978)
4. Barnsley, M.F., Rising, H.: Fractals Everywhere. Morgan Kaufmann, Burlington (2000)
5. Breban, R., Nusse, H.E.: On the creation of Wada basins in interval maps through fixed point tangent bifurcation. Phys. D: Nonlinear Phenom. **207**(1–2), 52–63 (2005). doi:10.1016/j.physd.2005.05.012
6. Cartwright, J.H.: Newton maps: fractals from Newton's method for the circle map. Comput. Gr. **23**(4), 607–612 (1999). doi:10.1016/S0097-8493(99)00078-3
7. Cayley, A.: Application of the Newton–Fourier method to an imaginary root of an equation. Q. J. Pure Appl. Math **16**, 179–185 (1879)
8. Chandra Sekhar, D., Ganguli, R.: Fractal boundaries of basin of attraction of Newton–Raphson method in helicopter trim. Comput. Math. Appl. **60**(10), 2834–2858 (2010). doi:10.1016/j.camwa.2010.09.040
9. Daza, A., Wagemakers, A., Sanjuán, M.A.F., Yorke, J.A.: Testing for Basins of Wada. Sci. Rep. **5**, 16,579 (2015). doi:10.1038/srep16579
10. Drexler, M., Sobey, I., Bracher, C.: On the fractal characteristics of a stabilised Newton method. Oxford University Computing Laboratory, Oxford (1995)
11. Drexler, M., Sobey, I., Bracher, C.: Fractal Characteristics of Newton's Method on Polynomials. Oxford University Computer Laboratory, Oxford (1996)
12. Epureanu, B.I., Greenside, H.S.: Fractal basins of attraction associated with a damped Newton's method. SIAM Rev. **40**(1), 102–109 (1998). doi:10.1137/S0036144596310033
13. Fedaravičius, A.P., Cao, M., Ragulskis, M.: Control of a dendritic neuron driven by a phase-independent stimulation. Chaos Solitons Fractals **85**, 77–83 (2016)
14. Frame, M., Neger, N.: Newton's Method and the Wada property: a Graphical Approach. Coll. Math. J. **38**(3), 192–204 (2007)
15. Gilbert, W.J.: Generalizations of Newton's method. Fractals **09**(03), 251–262 (2001). doi:10.1142/S0218348X01000737
16. Holt, R., Schwartz, I.: Newton's method as a dynamical system: global convergence and predictability. Phys. Lett. A **105**(7), 327–333 (1984). doi:10.1016/0375-9601(84)90273-1
17. Huber, P.J.: Robust Statistics. Springer, Berlin (2011)
18. Straffin Jr., P.: Newton's method and fractal patterns. Applications of Calculus **3**, 68–84 (1991)
19. Kennedy, J., Yorke, J.A.: Basins of Wada. Phys. D **51**(1–3), 213–225 (1991). doi:10.1016/0167-2789(91)90234-Z
20. Krause, E.F.: Taxicab Geometry: An Adventure in Non-Euclidean Geometry. Courier Corporation, Mineola (1975)
21. Landauskas, M., Ragulskis, M.: Clocking convergence to a stable limit cycle of a periodically driven nonlinear pendulum. Chaos: Interdisc. J. Nonlinear Sci. **22**(3), 033,138 (2012)
22. Nusse, H.E., Yorke, J.A.: Wada basin boundaries and basin cells. Phys. D **90**(3), 242–261 (1996). doi:10.1016/0167-2789(95)00249-9
23. Ott, E.: Chaos in Dynamical Systems. Cambridge University Press, Cambridge (2002)
24. Poon, L., Campos, J., Edward, O., Grebogi, C.: Wada basin boundaries in chaotic scattering. Int. J. Bifurc. Chaos **06**(02), 251–265 (1996). doi:10.1142/S0218127496000035
25. Portela, S., Iber, E.: Fractal and Wada exit basin boundaries in tokamaks. Int. J. Bifurc. Chaos **17**(11), 4067–4079 (2007). doi:10.1142/S021812740701986X
26. Sarkar, N., Chaudhuri, B.: An efficient differential box-counting approach to compute fractal dimension of image. IEEE Trans. Syst. Man Cybern. **24**(1), 115–120 (1994)

27. Schröder, E.: Ueber unendlich viele Algorithmen zur Auflösung der Gleichungen. Math. Ann. **2**(2), 317–365 (1870). doi:10.1007/BF01444024
28. Sobey, I.J.: Characteristics of Newton's method on polynomials. Oxford Computer Lab, Oxford (1996)
29. Susanto, H., Karjanto, N.: Newton's method's basins of attraction revisited. Appl. Math. Comput. **215**(3), 1084–1090 (2009). doi:10.1016/j.amc.2009.06.041
30. Sweet, D., Ott, E., Yorke, J.A.: Topology in chaotic scattering. Nature **399**(6734), 315–316 (1999). doi:10.1038/20573
31. Vandermeer, J.: Wada basins and qualitative unpredictability in ecological models: a graphical interpretation. Ecol. Model. **176**(1–2), 65–74 (2004). doi:10.1016/j.ecolmodel.2003.10.028
32. Vandermeer, J., Stone, L., Blasius, B.: Categories of chaos and fractal basin boundaries in forced predator–prey models. Chaos Solitons Fractals **12**(2), 265–276 (2001). doi:10.1016/S0960-0779(00)00111-9
33. Walsh, J.: The dynamics of Newton's method for cubic polynomials. Coll. Math. J. **26**, 22–28 (1995)
34. Wang, X., Yu, X.: Julia sets for the standard Newton's method, Halley's method, and Schröder's method. Appl. Math. Comput. **189**(2), 1186–1195 (2007). doi:10.1016/j.amc.2006.12.002
35. Zhang, Y., Luo, G.: Unpredictability of the Wada property in the parameter plane. Phys. Lett. A **376**(45), 3060–3066 (2012). doi:10.1016/j.physleta.2012.08.015
36. Zhang, Y., Luo, G.: Wada bifurcations and partially Wada basin boundaries in a two-dimensional cubic map. Phys. Lett. A **377**(18), 1274–1281 (2013). doi:10.1016/j.physleta.2013.03.027